The strength of alpha-beta oscillatory coupling predicts motor timing precision

Laetitia Grabot, Tadeusz W. Kononowicz, Tom Dupré La Tour, Alexandre Gramfort, Valérie Doyère, Virginie van Wassenhove

Behavioral/Cognitive

The Strength of Alpha–Beta Oscillatory Coupling Predicts Motor Timing Precision

Laetitia Grabot,[1]* Tadeusz W. Kononowicz,[1]* Tom Dupré la Tour,[2] Alexandre Gramfort,[2,3,4] Valérie Doyère,[5] and Virginie van Wassenhove[1]

[1]Cognitive Neuroimaging Unit, CEA DRF/Joliot, INSERM, Université Paris-Sud, Université Paris-Saclay, NeuroSpin center, 91191 Gif-sur-Yvette, France, [2]LTCI, Telecom ParisTech, Université Paris-Saclay, 75013 Paris, France, [3]Inria, Université Paris-Saclay, Saclay, 91120 Palaiseau, France, [4]CEA, Université Paris-Saclay, 91191 Gif-sur-Yvette, France, and [5]Neuro-PSI, Université Paris-Sud, Université Paris-Saclay, CNRS, 91405 Orsay, France

Precise timing makes the difference between harmony and cacophony, but how the brain achieves precision during timing is unknown. In this study, human participants (7 females, 5 males) generated a time interval while being recorded with magnetoencephalography. Building on the proposal that the coupling of neural oscillations provides a temporal code for information processing in the brain, we tested whether the strength of oscillatory coupling was sensitive to self-generated temporal precision. On a per individual basis, we show the presence of alpha– beta phase–amplitude coupling whose strength was associated with the temporal precision of self-generated time intervals, not with their absolute duration. Our results provide evidence that active oscillatory coupling engages α oscillations in maintaining the precision of an endogenous temporal motor goal encoded in β power; the *when* of self-timed actions. We propose that oscillatory coupling indexes the variance of neuronal computations, which translates into the precision of an individual's behavioral performance.

Key words: alpha; beta; cross-frequency coupling; phase–amplitude coupling; time perception; timing

Significance Statement

Which neural mechanisms enable precise volitional timing in the brain is unknown, yet accurate and precise timing is essential in every realm of life. In this study, we build on the hypothesis that neural oscillations, and their coupling across time scales, are essential for the coding and for the transmission of information in the brain. We show the presence of alpha– beta phase–amplitude coupling (α–β PAC) whose strength was associated with the temporal precision of self-generated time intervals, not with their absolute duration. α–β PAC indexes the temporal precision with which information is represented in an individual's brain. Our results link large-scale neuronal variability on the one hand, and individuals' timing precision, on the other.

Introduction

Assessing how the brain precisely keeps track of time is typically complicated when using sensory stimulation, which prevents disentangling endogenous timing brain processes from exogenous or sensory-driven processes. Using a temporal production task (Mita et al., 2009) helps to bypass this difficulty: participants self-initiate their endogenous timing by pressing a button, and press a second time when they considered that the required duration has elapsed. The two actions are internally generated and driven by an endogenous timing goal independently of any sensory inputs. Recording brain activity between the two button presses may provide insights on how the brain endogenously computes time, and self-generates a duration. As in many daily activities, the goal of reliable temporal production in this task consists in being accurate (i.e., minimizing the constant error) and precise (i.e., minimizing the variance).

Here, we explored the role of neural oscillations during the generation of a time interval in the absence of exogenous stimulation, and tested whether the coupling of neural oscillations was a signature of the temporal accuracy and/or precision of timed actions. The relevance of neural oscillations for cognitive opera-

Received Sept. 25, 2018; revised Nov. 23, 2018; accepted Dec. 16, 2018.

Author contributions: L.G., T.W.K., and V.v.W. designed research; L.G., T.W.K., and V.v.W. performed research; L.G., T.W.K., T.D.l.T., A.G., and V.v.W. analyzed data; L.G. and T.W.K. wrote the first draft of the paper; L.G., T.W.K., A.G., V.D., and V.v.W. edited the paper; L.G., T.W.K., V.D., and V.v.W. wrote the paper.

This work was supported by the Paris-Saclay IDEX NoTime to V.D., A.G., and V.v.W., the ERC Starting Grant MINDTIME ERC-YStG-263584 Grant to V.v.W., the ERC Starting Grant SLAB ERC-YStG-676943 to A.G., and the ANR-16-CE37-0004-04 AutoTime to V.D. and V.v.W. The funders had no role in study design, data collection and analysis, decision to publish, or preparation of this paper. Preliminary results of this work were presented at the *International Cognitive Neuroscience* workshop (Amsterdam, Netherlands, 2017). We thank Nancy Kopell for her astute comments on an earlier version of the paper.

The authors declare no competing financial interests.

*L.G. and T.W.K. contributed equally to this work.

Correspondence should be addressed to Tadeusz W. Kononowicz at t.w.kononowicz@icloud.com or Laetitia Grabot at laetitia.grabot@gmail.com.

https://doi.org/10.1523/JNEUROSCI.2473-18.2018

tions is largely acknowledged (Buzsáki and Draguhn, 2004; Jensen and Colgin, 2007; Fries, 2015) and cross-frequency coupling (Canolty and Knight, 2010) may support long-range communication and integration over distinct spatial and temporal scales (Akam and Kullmann, 2014; Fries, 2015). A common form of oscillatory nesting is the modulation of high-frequency power [e.g., gamma (γ)] by the phase of low-frequency oscillations [e.g., theta (θ)]. Robust phase–amplitude coupling (PAC) has been described (Tort et al., 2008, 2009) and may be involved in the representation of temporal sequences (Heusser et al., 2016), implicated in working memory (Axmacher et al., 2010; Voytek et al., 2010; Lisman and Jensen, 2013; Roux and Uhlhaas, 2014) and in speech processing (Canolty et al., 2006; Giraud and Poeppel, 2012). Additionally, the observation that low-frequency oscillations regulate spike timing in the human brain raised the hypothesis that PAC may provide a temporal code for cognition (Jacobs et al., 2007; Buzsáki, 2010), but whether such temporal code influences temporal cognition is unknown. Using a temporal production task was expected to provide novel insights on this question.

Oscillatory coupling could mediate the integration of information across temporal scales during interval timing (Gu et al., 2015) so that higher-frequency activity would presumably integrate over the time scales of low-frequency neural activity (van Wassenhove, 2016). The information-theoretic internal clock (Treisman, 1963, for review see Kononowicz and van Wassenhove, 2016) implies that duration estimation results from the integration of information (i.e., a count of number of pulses or events) over time: the high-frequency activity would thus index pulses generated by the pacemaker, whereas low-frequency oscillations would implement the gating and accumulation of pulses. A stronger PAC would result in optimal integration of information, and linearly predict the generated duration. Alternatively, oscillatory coupling may implement the maintenance of task-relevant information in working memory (Roux and Uhlhaas, 2014), which would predict a linear association with precision. PAC may regulate the precision of information during its maintenance over relevant brain networks. We thus investigated whether the temporal precision of motor timing, i.e., the precision of self-generated time intervals, rely on the temporal optimization of neural information through oscillatory coupling mechanisms.

To contrast the integration and the precision working hypotheses, we related three distinct aspects of timing behavior with oscillatory activity recorded with magnetoencephalography (MEG): performance (the produced duration), accuracy (the variation of the temporal production relative to the target interval, or constant error), and precision (the variance of temporal production across trials). The endogenous generation of a time interval was characterized by robust alpha–beta (α–β) PAC observable on a per individual basis. Crucially, the strength of α–β coupling correlated with timing precision, but not with the produced duration itself. Our results support the fundamental role of oscillatory coupling in the temporal coding of information, extending this notion to self-generated timing and behavioral precision.

Materials and Methods

Participants. Nineteen right-handed volunteers (11 females, mean age: 24 years old) with no self-reported hearing/vision loss or neurological pathology took part in the experiment and received monetary compensation for participation. Each participant provided a written informed consent in accordance with the Declaration of Helsinki (2008) and the Ethics Committee on Human Research at NeuroSpin (Gif-sur-Yvette). The data of seven participants could not be included in the analysis because of the absence of anatomical MRI, problems with the head positioning system, abnormal artifacts during MEG recordings, and two participants did not finish the experiment. These datasets were excluded a priori and were not visualized or inspected. Importantly, this harsh procedure did not affect the reliability and power of our statistical assessment as most analyses were performed per block, in which a sample for one observation corresponded to ~100 experimental trials. Additionally, we assessed the power of the linear mixed design where precision was predicted by the α–β PAC, which is the main effect reported in the paper. We performed power analysis using Monte Carlo simulation with 1000 samples, alpha = 0.05, effect size = 90 (i.e. equal to the effect size reported in this paper) using the *simr* R package. For these parameters, the simulation showed 88% of power, where 80% is considered to be sufficient in the literature (Green and MacLeod, 2016). To sum up, this simulation showed that the power in the current study is just in the required range. Hence, the final sample comprised 12 participants (7 females, mean age: 24). All but two participants performed six experimental blocks (1 block was removed for 2 participants because of excessive artifacts or lack of conformity to task requirements).

Stimuli and procedure. Before the MEG acquisitions, participants were acquainted with the task by producing 1.45 s duration intervals, and reading written instructions explaining the full experimental procedures. A single trial consisted in producing a time interval followed by the self-estimation of the produced time interval. Feedback varied across blocks (Blocks 1 and 4 included 100% feedback; Blocks 2, 3, 5, and 6 included 15% feedback). Each trial started with the presentation of a "+" sign on the screen indicating to participants they could initiate an interval whenever they decided to (Fig. 1*A*). Participants initiated their production of the time interval with a brief button press (R1) when they felt ready to start, and terminated it with another brief button press (R2) when they considered that 1.45 s had elapsed. To initiate and terminate their time production, participants were asked to press the top button on a Fiber Optic Response Pad (FORP; Science Plus Group) using their right thumb. The "+" sign was removed from the screen during the estimation of the time interval to avoid any sensory cue or confounding responses in brain activity related to the production of the timed interval. Following the production of the time interval, participants were asked to self-estimate their time estimation using a continuous scale identical to the one used to provide feedback. The intertrial interval between the end of the self-estimation and the first cursor display ranged between 1 and 1.5 s.

Following the completion of the time interval, participants received feedback. A row of five symbols indicated the objective category of the time production tailored to each individual's time estimation. The feedback range was set to the value of the perceptual threshold estimated on a per individual basis during a task performed before MEG acquisition (mean population threshold = 0.223 s, SD = 0.111 s). A near correct time production yielded the middle "~" symbol to turn green; a too short or too long time production turned the symbols "−" or "+" orange, respectively; a time production that exceeded these categories turned the symbols "− −" or "+ +" red. In Block 1, feedback was provided in all trials. In Blocks 2–5, feedback was randomly assigned to 15% of the trials. In Blocks 4 to 6, the target duration was increased to 1.45 s + (individual threshold/2). Feedback was presented in all trials in Block 4 and in 15% of trials in Block 5 and 6, This experimental manipulation was outside the scope of the question in this study, and was addressed in another analysis assessing the possibility of implicit temporal recalibration (cf. Kononowicz et al., 2018). On average, the new target duration was 1.56 s based on the average threshold. In Blocks 1 and 4, participants produced 100 trials; in Blocks 2, 3, 5, and 6, participants produced 118 trials.

Between all experimental blocks, participants were reminded to produce the 1.45 s target duration as accurately as possible, and to maximize the number of correct trials in each block. Note that the manipulation of feedback was investigated in a different set of analyses pertaining to temporal metacognition during motor timing (Kononowicz et al., 2018) and does not constitute our condition of interest in this study.

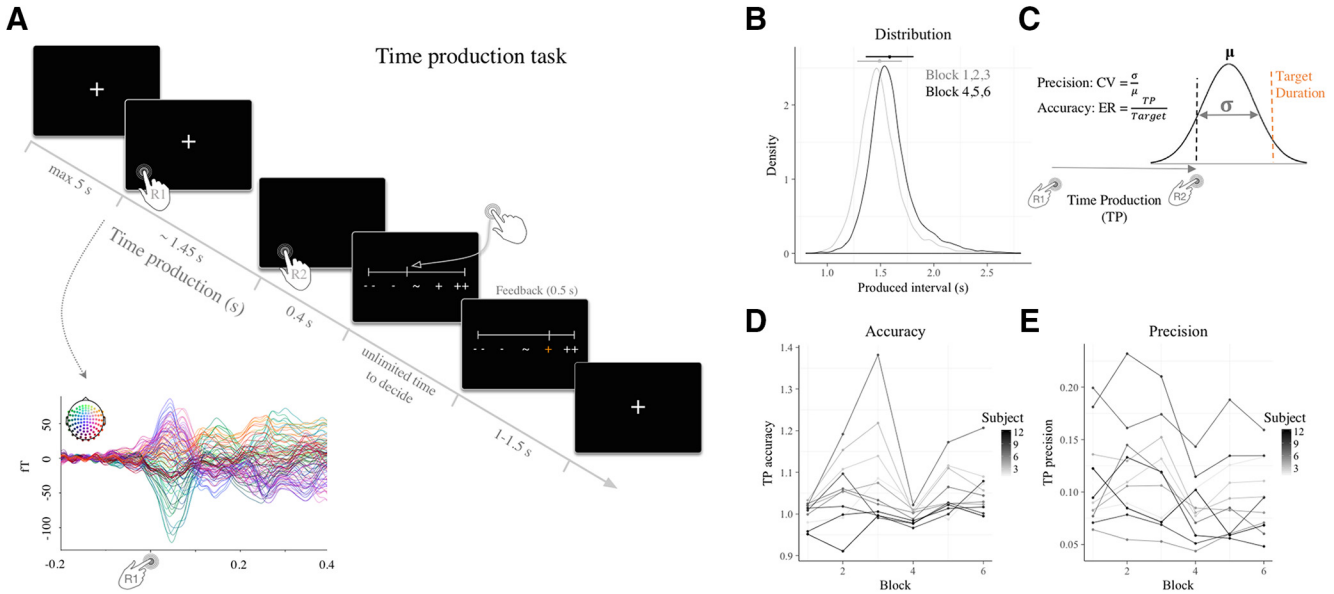

Figure 1. Probing behavioral precision (CV) and accuracy (ER) using a time production paradigm. ***A***, Time course of an experimental trial. Participants received feedback on their performance for all trials in Blocks 1 and 4, and for 15% of trials in Blocks 2, 3, 5, and 6. The inset plot depicts the evoked MEG responses locked to R1. ***B***, Probability density function of all TP when producing 1.45 s (gray) and 1.56 s (black). The dots and bars indicate their respective means and SD. ***C***, Schematic depiction of how temporal precision and accuracy were quantified. The black dotted line depicts an example of a produced time interval drawn from a Gaussian distribution of produced intervals (solid black curve; mean μ and SD σ). The next panels plot the precision and the accuracy across blocks and participants. ***D***, Accuracy in time production computed as ER (= production/target) per block and per individual (dot). The accuracy of TP did not significantly change in the course of the experiment. ***E***, Temporal precision computed as CV over time productions per block and per individual (dot). The temporal precision of TP did not significantly change in the course of the experiment.

Simultaneous MEG/EEG recordings. The experiment was conducted in a dimly lit magnetically-shielded room located at NeuroSpin (CEA/DRF/Joliot) in Gif-sur-Yvette. Participants sat in an armchair with eyes opened looking at a projector screen. Electromagnetic brain activity was recorded using the whole-head Elekta Neuromag Vector View 306 MEG system equipped with 102 triple-sensors elements (2 orthogonal planar gradiometers, and 1 magnetometer per sensor location) and the 64 native EEG system using Ag-AgCl electrodes (EasyCap) with impedances <15 kΩ. Participants' head position was measured before each block using four head-position coils placed over the frontal and the mastoid areas. The four head-position coils and three additional fiducial points (nasion, left and right pre-auricular areas) were digitized using a 3D digitizer (Polhemus) for subsequent coregistration of the individual's anatomical MRI with brain recordings. MEG and EEG recordings were sampled at 1 kHz, and bandpass filtered between 0.03 and 330 Hz. The electro-oculograms (horizontal and vertical eye movements), electrocardiograms, and electromyograms were simultaneously recorded. Feedback was presented using a PC running Psychtoolbox software (Brainard, 1997) in MATLAB (R2012, Mathworks).

Data analysis

MEG/EEG data preprocessing. MEG data were low-passed at 160 Hz, decimated at 333 Hz and epoched from −1.2 to 2 s around the first button press (R1). Epochs were rejected if signal amplitudes exceeded 4 fT/cm for gradiometers and 5500 fT for magnetometers. Baseline correction was applied by subtracting the mean value ranging from −0.2 to 0 s before R1.

Power density spectrum analysis. The power spectrum density (PSD) was computed using Welch's method, between 1 and 45 Hz, with 0.8 s length tapers, on a window from 0.4 to 1.2 s. PSD were averaged across all magnetometers, conditions and participants.

PAC calculation and statistical assessment. Our analysis of PAC conducted in sensor space exclusively focused on activity recorded with magnetometers; PAC in source space included all sensors (magnetometers, gradiometers, EEG electrodes). We selectively used magnetometers in sensor space for simplicity of interpretation in topographies. Signal source separation in preprocessing stages alleviate the independence of gradiometers and magnetometers; gradiometers would also need to be combined as pairs to make physiological sense and would implicate additional difficulties in the computation of phase coupling. We thereafter use the word "sensors" to refer to magnetometers.

To prevent the contamination of the timed interval from both R1- and R2-evoked responses, we solely focused on the time segment from 0.4 to 1.2 s following R1. PAC was assessed using the modulation index (MI; Tort et al., 2009); namely, the fully epoched data were first bandpass filtered (slow-frequency bandwidth = 2 Hz, high-frequency bandwidth = 20 Hz), and then the instantaneous amplitude of the high-frequency and the phase of the slow-frequency were extracted from the Hilbert transform applied to the epoch data. The data were then segmented into 0.4 to 1.2 s epochs. To assess whether the distributions diverged from uniformity, the Kullback–Leibler (KL) distance was calculated then normalized to give the MI. The KL distance was estimated between histograms with 18 bins. The slow-frequency component ranged from 3.5 to 14.1 Hz (step by 0.2 Hz) and the high-frequency range was from 14 to 160 Hz (in step of 2 Hz). A comodulogram was computed for each sensor.

Visual inspection of grand average data across all individuals and sensors revealed a strong MI between the phase of α oscillations and the power of β oscillations. To assess the statistical significance of PAC at the individual level, the MI was compared with a surrogate distribution (n = 100) computed by shifting the low-frequency signal by a minimum of 1 s, as has been previously proposed (Tort et al., 2010). To reduce computational demands, this procedure was only performed on 10 selected sensors per individual, based on the maximal α–β MI value (8–12/15–40 Hz) across all conditions. It should however be noticed that the selection process is independent from the main contrasts-of-interest concerning behavioral accuracy and precision. A Z-score was calculated for each of the 10 selected sensors and a Z-score >4 (i.e., $p = 3e{-}5$) was reported as significant.

The problem of multiple comparisons while computing PAC has been rarely discussed or acknowledged. We note that controlling for multiple comparisons would necessitate correction of 0.05 by 3869 (number of cells in the MI matrix) × 102 (number of sensors) number of comparisons, which would result in 1.27.e−7 (i.e., Z-score of 5.28). Sufficient evidence for PAC not confounded by multiple-comparisons problem can be gathered by inspection of the Z-score values in Figure 3*A*, which reached values >20th Z-score corresponding to 5.6e−89 p value.

To assess whether PAC was specific to time production, we compared the MI computed during baseline from −0.8 to 0 s before R1 to the MI computed during the produced interval (0.4 to 1.2 s). Because participants were allowed to begin the task when ready after the display of the cross, we selected trials with at least 1.1 s between the cross onset and the first button press (R1) to avoid any contamination of visual-evoked activity. On average 90 ± 80 trials were retained. For three participants, the number of trials was not sufficient to compute a reliable MI (6, 15, and 21 trials). Nevertheless, the cluster-based permutation *t* test was run on all individuals and similar results held when the same analysis was performed on nine participants.

Crucially, because of methodological limitations inherent to the filtering process, PAC can only be established for a driver's frequency that is above twice the frequency of the high-frequency oscillations. To insure that the α and β frequencies involved in the oscillatory coupling were not harmonically related, we extracted, per individual, the α and β frequencies corresponding to the maximal MI averaged across the 10 selected sensors of each participant. We then ran a paired *t* test between the β frequency and the second harmonic of the α frequency to insure that the coupling was not spurious. The outcomes of these analyses are detailed in Results.

MEG/EEG-aMRI coregistration. Anatomical magnetic resonance imaging (aMRI) was used to provide high-resolution structural images of each individual's brain. The anatomical MRI was recorded using a 3-T Siemens Trio MRI scanner. Parameters of the sequence were as follows: voxel size: 1.0 × 1.0 × 1.1 mm; acquisition time: 466 s; repetition time = 2300 ms; and echo time = 2.98 ms. Volumetric segmentation of participants' anatomical MRI and cortical surface reconstruction was performed with the FreeSurfer software (http://surfer.nmr.mgh.harvard.edu/). A multiecho FLASH pulse sequence with two flip angles (5° and 30°) was also acquired (Fischl et al., 2004; Jovicich et al., 2006) to improve coregistration between EEG and aMRI. These procedures were used for group analysis with MNE software (Gramfort et al., 2013, 2014). The coregistration of the MEG/EEG data with the individual's structural MRI was performed by realigning the digitized fiducial points with MRI slices. To ensure reliable coregistration, an iterative refinement procedure was used to realign all digitized points with the individual's scalp.

MEG source reconstruction for PAC analysis. To compute PAC at the source level, single-trial time series were projected into source space. All three types of sensors were combined: magnetometers, gradiometers, and EEG signals. Before the main source reconstruction, individual forward solutions for all source locations on the cortical sheet were computed using a three-layer boundary element model constrained by the individual's anatomical MRI. Cortical surfaces extracted with FreeSurfer were downsampled to 10,242 equally-spaced sources on each hemisphere (3.1 mm between sources). The noise covariance matrix for each individual was estimated using baseline activity (interval from −0.2 to −0.1 s relative to R1). The forward solution, the noise covariance and source covariance matrices were used to calculate the dSPM estimates (Dale et al., 2000). The inverse computation was done using a loose orientation constraint (loose = 0.2, depth = 0.8) on the radial component of the signal. Individuals' current source estimates were registered on the FreeSurfer average brain for surface-based analysis and visualization. Once time-resolved activity was reconstructed in cortical space, we used the "aparc" parcellation from FreeSurfer to define cortical labels (Desikan–Killiany atlas; Desikan et al., 2006). Given the large number of dipoles within a label, and to reduce computational demands, we reduced each label to five vertices based on either maximal α or β power, so that the selection process was independent of PAC. We then computed PAC for each of these selected vertices and averaged it for each label. The correlation analyses were then carried on these selected vertices. As seen in Figures 3*C* and 9*C*, both selections yielded very comparable results. To prevent signal cancelation originating from different dipoles, the label time courses were treated as single trials for PAC computation.

Experimental conditions and correlation analyses. Analyses were performed on the basis of objective performance in time production classified as short, intermediate, or long separately for each experimental block. Computing these three conditions within a block focused the analysis on local variations of brain activity as a function of the observed participant's performance with respect to the mean temporal production of each participant. Epochs were concatenated across all six blocks for the analyses based on time production performance. The number of trials was equalized between short, intermediate and long conditions, leading to 168 trials (SD = 58) per condition. Additionally, the correlational analyses investigating precision and accuracy of timing processes was also extended to a per block analysis to gain a better insight of the fluctuation of these behavioral components over time. Precision was computed as coefficient of variation (CV) over time production on a per-block and per-participant basis. The CVs were calculated by dividing the SD by the mean duration production. Accuracy was quantified by the error ratio (ER): ERs were calculated by dividing the mean temporal production in a given set of data by the target interval in that set. It is important to note that precision and accuracy provide two distinct insights on individuals' temporal production. Although precision is uniquely described in reference to each individual's temporal production, the accuracy is computed in reference to the objective target duration. As such, both measures are complementary and not necessarily correlated. The target duration was 1.45 s in the first three blocks and 1.56 s in the last three blocks.

The sensor-level analyses were performed using linear mixed-effect (LME) models and model comparison to check whether factors other than PAC were needed to explain motor timing behavior. Correlational analyses of source estimates were performed for illustrative purposes and thus, we used nonparametric Spearman's for each label. All statistical analyses were performed in R v3.3.2 statistical programming language (R Core Team, 2016). For illustrative purposes, correlations in cortical space were computed using Spearman correlations. Bayesian ANOVA (Rouder et al., 2012) was performed using *BayesFactor* R package.

Calculating precision and accuracy metrics and accounting for inflated degrees of freedom. As described above, both precision (CV) and accuracy (ER) metrics were computed separately per block and per participant. As splitting the data per block and per individual could inflate the degrees of freedom, we used LME models (Pinheiro and Bates, 2000; Gelman and Hill, 2007), which, by default, accounted for individual, multiple per-subject observations in the data. For all regression analyses of sensor data, we used LME models. LMEs are regression models that model the data by taking into consideration multiple levels. Subjects and blocks were entered in the model as random effects that were allowed to vary in their intercept. *P* values were calculated based on a type-3 ANOVA with Satterthwaite approximation of degrees of freedom, using *lmerTest* package in R (Kuznetsova et al., 2017). The mixed-effects models approach was combined with model comparison, which allowed for evaluating the best fitting model in a systematic manner.

Data standardizing for regression model. As regression tests require a Gaussian distribution of the data, wherever applicable, and on the basis of Shapiro–Wilk normality test, the data were transformed using the Lambert W function. The Lambert W function provides an explicit inverse transformation, which removes heavy tails from the observed data (Goerg, 2011, 2015). First, the data were transformed into a heavy-tailed form using log-likelihood decomposition. Subsequently the heavy-tailed form was transformed back into a Gaussian distribution. All transformations were performed using *LambertW* R package.

Results

Behavioral evidence for variable precision and accuracy

Twelve participants were asked to produce a target interval by pressing a button at the start (R1) and at the end (R2) of their time production (TP; Fig. 1*A*). The target interval was 1.45 s in the first three experimental blocks, and 1.56 s in the last three experimental blocks. Participants complied with the task requirements by producing, respectively, 1.513 and 1.614 s time intervals (Fig. 1*B*). Although the overall performance was quite accurate, the time production data showed large variability both within-individuals (across blocks) and across individuals (Fig. 1*D*,*E*). This variability was quantified by the CV (Fig. 1*E*) and by the ER

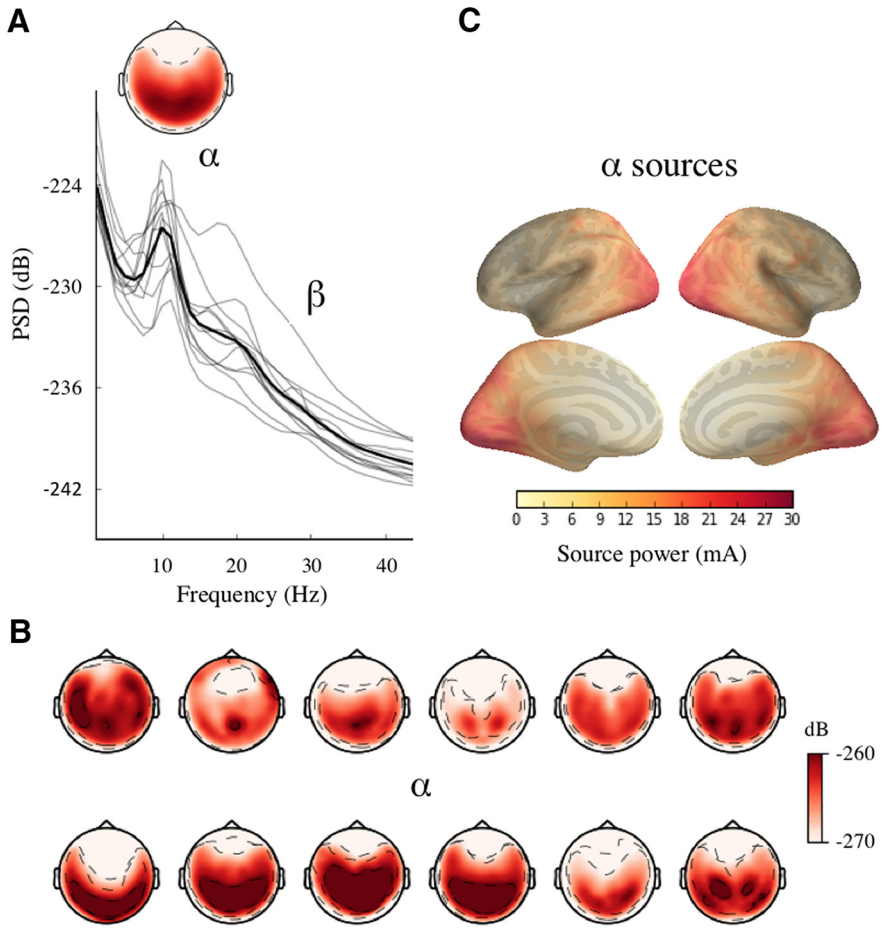

Figure 2. Oscillatory power in brain activity during time production. ***A***, The PSD was computed during the produced interval (0.4–1.2 s) and averaged across sensors, conditions and participants. The average PSD (thick line) across individuals (gray lines) showed a clear peak 10 Hz. The topo map shows the PSD averaged between 8 and 12 Hz. ***B***, The individual topographic maps for PSD. ***C***, Grand-average cortical source estimations revealed an occipito-parietal distribution of the oscillatory power.

(Fig. 1*D*): the CV was calculated by dividing the SD by the mean duration production, and the ER by dividing the mean time estimates by the target interval in a given block (Fig. 1*C*). The CV was thus a measure of precision, and the ER, a measure of accuracy. Both metrics were calculated per experimental block and per participant. Although changes in feedback were manipulated in the experimental design, there was no *ad hoc* hypothesis regarding its effects on possible PAC, notably because no significant changes in precision were found as a function of feedback (repeated-measures ANOVA; $F_{(5,65)} < 1$, $p > 0.1$). Additionally, as can be seen in Figure 1*D*, a general trend for a lengthening in duration estimation was observed over the entire course of the recording (repeated-measures ANOVA; $F_{(5,65)} = 2.71$, $p = 0.028$); this drift was shown to be independent from changes in feedback or duration (Kononowicz et al., 2018). In the next section, we explore the role of oscillatory coupling in timing.

Robust α–β coupling during time production

Before proceeding with PAC estimations, we assessed the PSD during the time interval from 0.4 to 1.2 s following R1 (to avoid motor-evoked responses) by averaging the PSD across all sensors, conditions, and individuals. A dominant peak was readily visible in the spectrum at α (~10 Hz) frequency, suggesting the existence of plausible regime for oscillatory coupling (Fig. 2*A*). The α peak was mainly localized in occipital and parietal regions (Fig. 2*B*,*C*).

To assess whether any form of PAC was present during the production of a time interval, we computed the MI (Tort et al., 2009) for all sensors from 0.4 to 1.2 s following the first button press R1. Visual inspection of grand average data across all individuals and all sensors revealed a strong MI between the phase of α oscillations and the power of β oscillations in centro-parietal sensors (Fig. 3*B*). For dimensionality reduction, we then selected 10 sensors displaying the maximal α–β MI on a per individual basis: as seen in Figure 3*A*, the 10 sensors with maximal α–β MI were mainly found in central and parietal regions for a majority of participants. For each of these selected sensors, the statistical significance of the MI was assessed at the individual level by shuffling the α phase (Tort et al., 2010). A Z-score >4 ($p < 0.0001$; Fig. 3*A* shows individual outlines) indicated that α–β PAC was statistically significant for each individual. Across participants, α–β MI was maximal for the phase of the 10.3 Hz peak frequency response (SD = 0.6), and for the amplitude of the 27.2 Hz peak frequency response (SD = 3.9). For a detailed report, Table 1 provides all individual frequency peak responses. Both the low- and high-frequency peak values were consistent with the individuals' α and β frequency peaks observed in the previous PSD (Figs. 2, 3; Table 1). Specifically, we observed that an individual's α peak frequency correlated with the α peak frequency of the individual's PAC ($r = 0.763$, $p = 0.004$; see Fig. 4).

Importantly, the β peak in α–β PAC was significantly distinct from the second harmonic of the α peak in the α–β PAC [$t = 7.064$, df = 11, $p < 0.001$; $CI_{95} = (4.5; 8.6)$], meaning that the observed α and β peak frequencies were not simply harmonics. Although this observation showed that the observed β activity was true neuronal activity (and not harmonics of α), it did not directly test whether PAC was artifactual. Later quantitative assessments testing the precision in temporal production will directly rule out the possibility that PAC is artifactual. To ensure the robustness of our observations, we confirmed these results with an alternative method to quantify α–β PAC capitalizing on a recently developed driven auto-regressive (DAR) statistical modeling approach (Dupré la Tour et al., 2017). DAR modeling revealed a comparable α–β PAC at the individual level (Figs. 3, 5).

To further assess which brain regions may exhibit the highest degree of coupling, we source-estimated PAC in cortex. First, we reconstructed the time-resolved signals on a single-trial basis, and used the same approach for PAC calculation as we did for the sensor data. We spatially defined brain regions using a predefined cortical parcellation (Desikan–Killiany atlas; Desikan et al., 2006) and reduced each label to five vertices showing maximal α power (see Material and Methods). α–β PAC was maximal in left sensorimotor regions, presumably because of the motoric components of the task (post-, pre-, para-central, and supramarginal

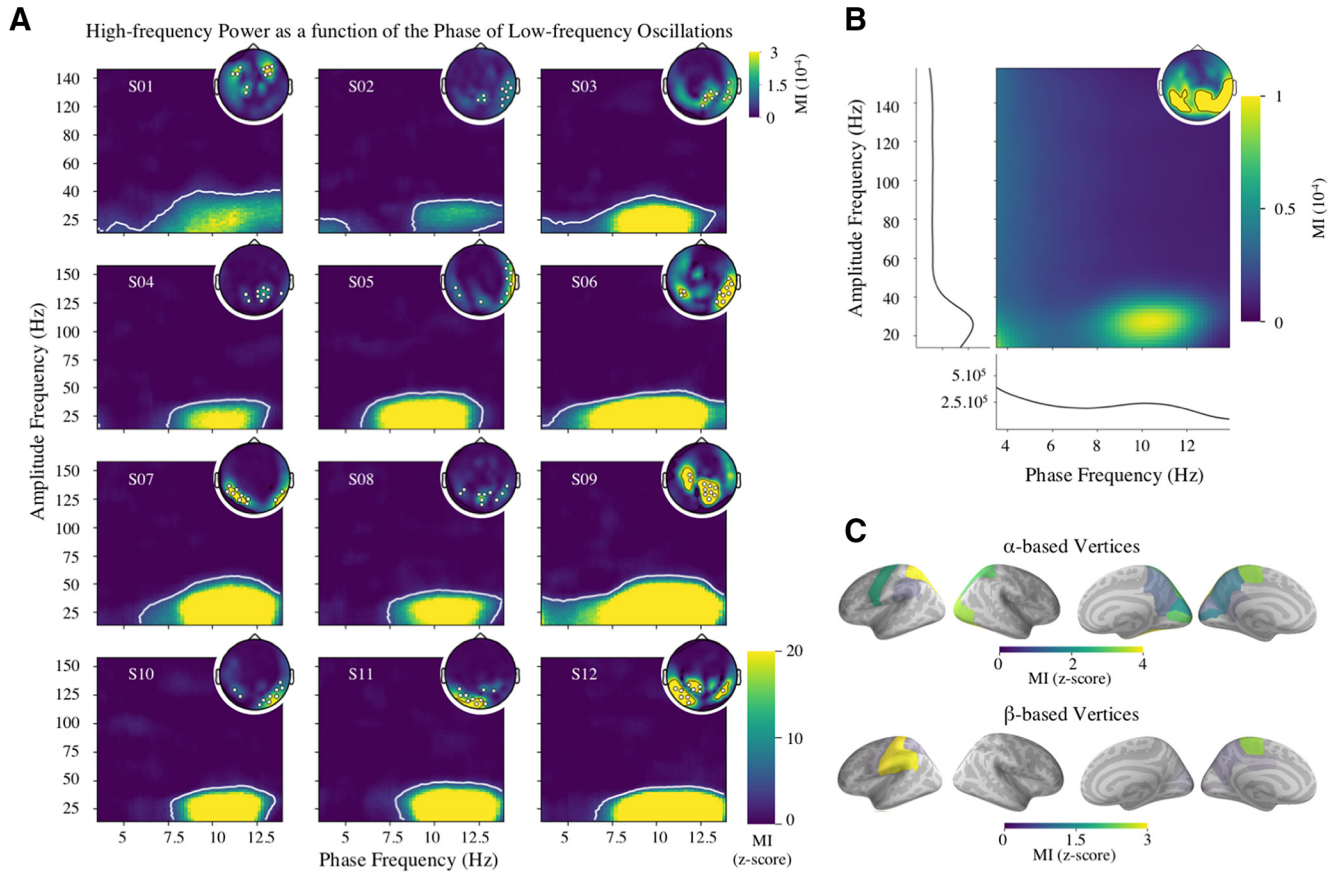

Figure 3. $\alpha-\beta$ PAC during time production. ***A***, Individual comodulograms showing the presence of significant $\alpha-\beta$ PAC as measured by the MI. The individual topographic maps (insets, top right; nose on top) provide the spatial distribution of the $\alpha-\beta$ MI observed at the scalp level: 10 sensors showing the highest MI (inset, white dots) were selected for the comodulogram. The white outlines on the individual comodulograms delineate significant *Z*-scored values (values >4, i.e., $p < 0.0001$). ***B***, Grand average comodulogram across all trials, all participants, and all sensors, showing significant $\alpha-\beta$ PAC. The average topographic map of the $\alpha-\beta$ MI (inset, top right) shares the same scale as in ***A***. ***C***, *Z*-score MIs were source-reconstructed in cortex. Brain regions showing maximal MI as computed on the basis of α (top) or β (bottom) power are reported.

Table 1. Individual α peak frequency extracted from the PSD and individual $\alpha-\beta$ PAC corresponding to their maximal MI

Participants	α Power peak, Hz	α PAC peak, Hz	β PAC peak, Hz
S01	9.40	9.1	18
S02	11.20	11.1	32
S03	9.70	9.9	28
S04	11.30	10.1	24
S05	9.50	9.7	26
S06	9.70	10.1	28
S07	12.30	10.9	30
S08	10.60	10.5	30
S09	10.90	10.5	32
S10	10.20	10.7	28
S11	11.20	10.7	26
S12	10.80	10.5	24

areas; Fig. 3*C*). High PAC was also found in parietal regions, in line with the notion that endogenous α rhythms would largely contribute to PAC. The α peak analysis (Fig. 2*C*) and the PAC source estimation (Fig. 3*C*) were thus topographically consistent with each other. To test the robustness of source estimations, we also conducted the analysis with a selection of spatial location based on the maximal β power: the left sensorimotor areas showed maximal $\alpha-\beta$ PAC, consistent with the α-based observations (Fig. 3*C*, bottom).

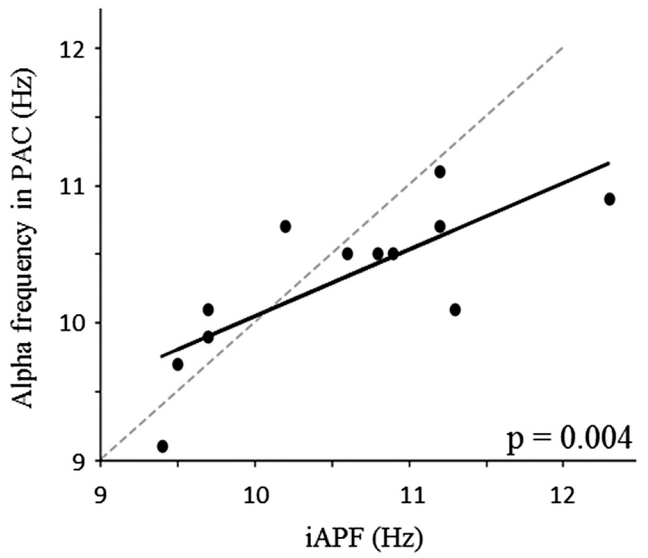

Figure 4. Individual α peak frequency (iAPF) correlates with α frequency observed in $\alpha-\beta$ PAC. To ensure that the α rhythm captured in the PSD (Fig. 2*A*) was involved in PAC computation, we correlated an individual α peak frequency with the frequency corresponding to each individual's maximal $\alpha-\beta$ MI ($r = 0.763$, $p = 0.004$).

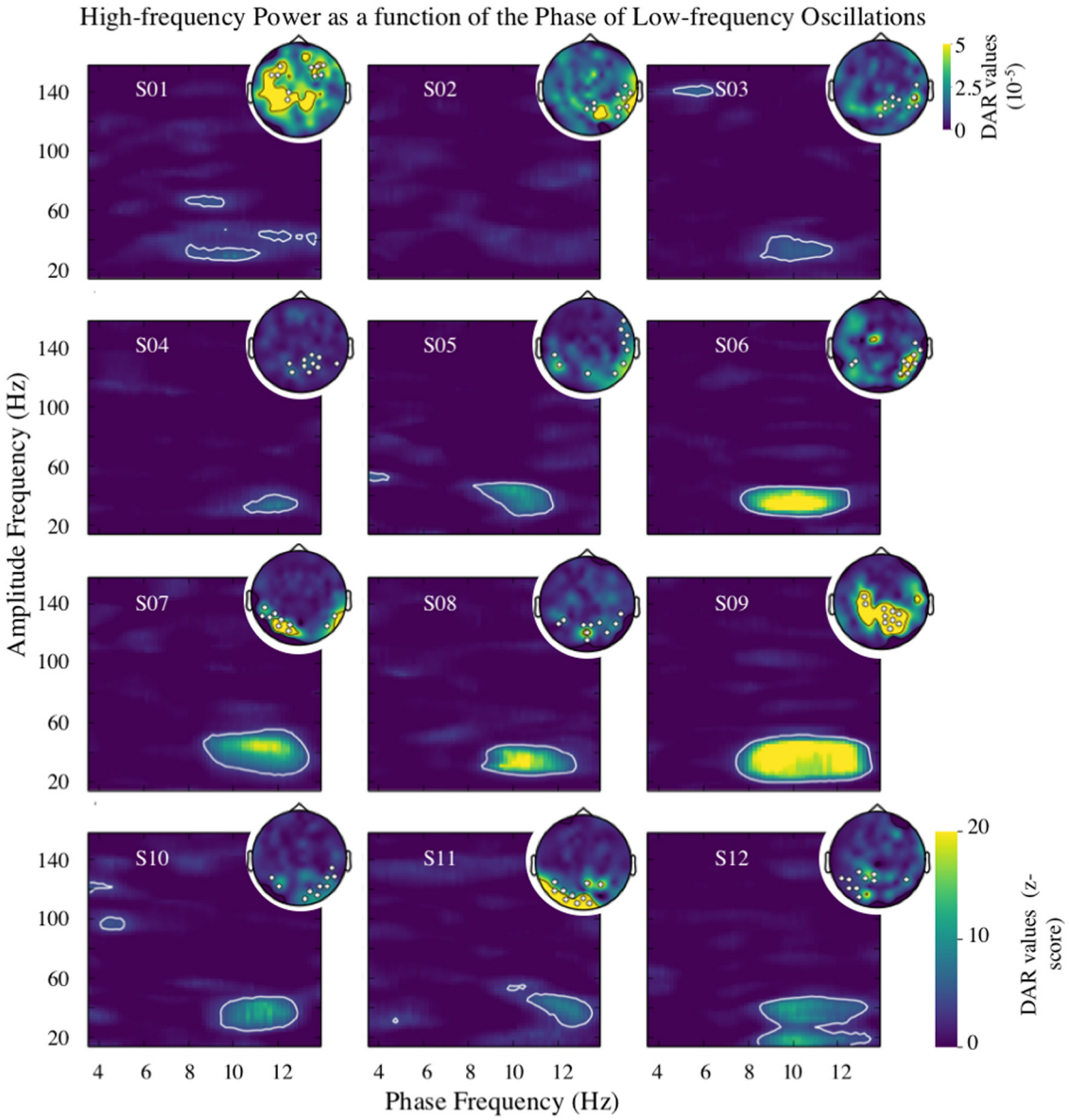

Figure 5. α–β PAC during time production computed with DAR model. We replicated the individual results of α–β PAC (Fig. 3*A*) using a novel DAR model (Dupré la Tour et al., 2017). The full comodulograms of *Z*-scored DAR values are plotted for each individual. Topographic maps of α–β DAR values are plotted in the right insets. The white contour corresponds to *Z*-score values >4 highlighting significant oscillatory coupling. In the DAR approach, and for consistency in comparing results, we kept the same set of sensors as in Figure 3*A*. For instance, in participant S02, the sensors showing maximal PAC with Tort's method (highlighted in white in the topographic inset) did not match with the sensors showing maximal PAC with DAR models; this spatial discrepancy explains why no significant α–β PAC is observed in the comodulogram of S02 despite significant coupling (yellow DAR values on the topographic insets). The DAR method provided a narrower focus on higher frequencies of power modulation, suggesting slightly larger specificity of high-power modulation. It is noteworthy that for both the Tort and the DAR methods, the peak of the high-frequency (Tort method = 27.2 Hz, SD = 3.9; DAR method = 34.5 Hz, SD = 2.3) were located in the vicinity of the β and lower γ frequencies. This suggests that for every α cycle at least one cycle of β was transiently modulated by the phase of α oscillation. As reported in Results, the peak frequencies for α and β found in the α–β PAC with the DAR method showed no harmonic relationship [$t = 18.641$, df = 11, $p < 0.001$, $CI_{95} = (11.1; 14.0)$].

α–β Coupling is specific to the interval being timed

Although we showed that α–β coupling was present during the production of temporal intervals, one may argue that the observed coupling was strictly relevant to motor preparation as opposed to motor timing. To test this, we capitalized on our experimental design, which required that participants self-initiated the production of the time interval: because participants volitionally initiated their first button press (R1) with no explicit time requirement or pressure, we used brain activity ranging from −0.8 s to R1 as a control for motor preparation. We tested whether the MI during the production of the time interval was significantly increased compared with this baseline brain response (before R1). A cluster-based permutation *t* test on comodulograms averaged across the selected sensors and across participants showed that α–β PAC was significantly larger during time production than during the volitional trial initiation ($p = 0.037$; Fig. 6). As the number of trials for PAC estimation was not optimal for three participants, the cluster permutation test was repeated for the nine participants with a sufficient number of trials for statistically robust estimation (>40 trials), confirming a PAC significantly larger than in baseline ($p = 0.016$). Importantly, because the power of the low-frequency oscillation may impact the MI (Dupré la Tour et al., 2017), we also insured that α power density did not differ before the time interval and during

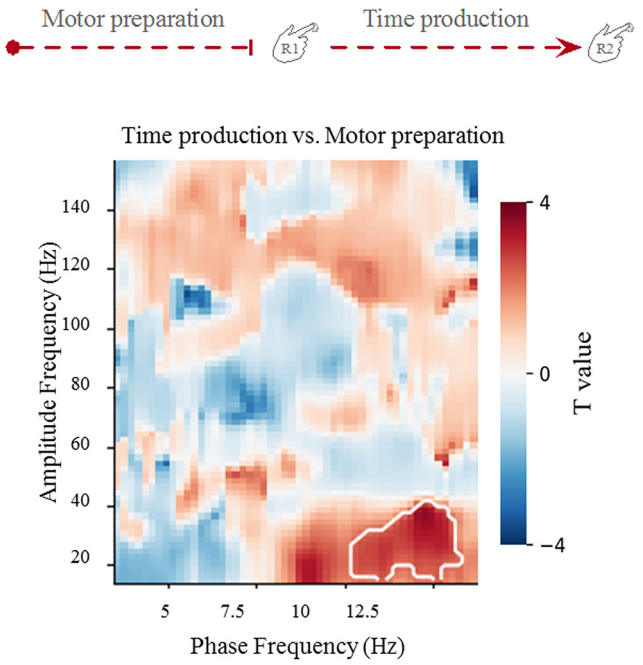

Figure 6. α–β PAC is specific to the timed interval R1–R2. To ensure that α–β coupling was related to endogenous timing processes, we contrasted PAC during temporal production (R1–R2 period) with PAC during the motor preparation to R1 of the same trial (−0.8 s to R1). All participants ($n = 12$) were included in this analysis. The strength of α–β PAC was significantly higher during the time production interval compared with motor preparation during the self-initiation of the time interval. The white line delineates a significant cluster corresponding to $p = 0.037$.

the production of the time interval ($p > 0.1$), and that the α–β power ratio did not significantly differ between these two time periods ($p > 0.1$). In sum, these controls showed that the α–β coupling could not be explained by a simple power difference between the two equivalent motor preparation time periods.

To put our findings in context, it is noteworthy that in a study requiring similar motor demands (de Hemptine et al., 2015), the strength of PAC was shown to decrease during motor preparation compared with the time period of the movement; here, during a timing task, we found the opposite pattern. Altogether, our comparisons against baseline showed that the observed α–β PAC was likely linked to the task requirements of endogenously producing a time interval, and thus that α–β PAC could play a functional role in temporal performance, which we explored next.

No monotonic associations between oscillatory coupling strength and time estimation

Under the first working hypothesis, if PAC mediated the integration of information across temporal scales during timing, the coupling strength would be associated with the length of the produced duration. To directly test whether the generation of a time interval resulted from the online integration of endogenous information mediated by oscillatory coupling, we investigated whether the strength of α–β PAC predicted timing behavior in an absolute manner between trials. For this, and in line with common practice (Kononowicz and Van Rijn, 2011), epochs were sorted as a function of participants' performance; namely, short, intermediate, or long duration productions. The α–β MI was averaged across selected sensors for each individual and for each produced duration (Fig. 7). A one-way repeated-measures ANOVA conducted with produced duration as factor (3 levels: short, intermediate, long) revealed no significant differences in the strength of α–β PAC as a function of duration ($F_{(2,11)} = 0.657$, $p = 0.528$). To further investigate the likelihood of the null hypothesis, we ran the same analysis with Bayesian ANOVA: a Bayes Factor of 0.29 indicated that the data were $1/0.29 = 3.4$ times more likely to occur under the null hypothesis than under the alternative hypothesis, providing "substantial" (Jeffreys, 1961) or "moderate" (Lee and Wagenmakers, 2014) evidence that the strength of α–β coupling were independent of absolute timing performance.

As no change in α–β coupling strength was found as a function of the produced time interval, we instead asked whether the phase relationship between α and β changed as a function of the produced time interval. To test this, epochs were locked on the peak of the α oscillations (Fig. 8) to compare whether maximal beta power (15–40 Hz) was found at different phase of the α oscillation as a function the produced time interval. No significant changes in the phase relationship between α and the β power were observed (Fig. 8*A*). Overall, we found that for four participants, an increase in β power occurred during the ascending slope of the α oscillation, and for the remaining eight participants, at the descending slope of the α oscillation. When looking at the individual α phase distribution at which β power was maximal for each duration category, a large interindividual variability could be observed (Fig. 8*B*). When comparing the mean phase relationship between α and β power during short and long temporal intervals, no significant differences were found ($t = 0.12$, $p = 0.91$; Fig. 8*C*).

Hence, and overall, the length of the temporal production did not significantly influence the strength or the phase relationship of α–β coupling. These observations land no substantial support for the direct implication of α–β PAC in time estimation *per se*, and we thus turned to our second working hypothesis.

The strength of α–β PAC indexes timing precision

Under the precision working hypothesis, oscillatory coupling may reflect the precision with which an endogenous timing goal may be maintained during motor production. To test this, we quantified how the observed α–β PAC related to participants' timing accuracy and precision. The α–β MI were averaged across sensors separately for each individual, and for each experimental block, and entered as predictors in two regression models; the precision (measured by CVs) and the accuracy (measured by ERs) models.

First, we found that the strength of α–β oscillatory coupling significantly predicted the behavioral CV ($t_{(64)} = 3.3$, $\beta = -89$, $p = 0.002$; Fig. 9*A*). The statistical analysis, based on Akaike information criterion (AIC; Wagenmakers and Farrell, 2004), showed that the model containing α–β PAC as predictor was justified compared with the model including only the intercept ($\Delta AIC = 7.5$, $p = 0.002$). Inclusion of the interaction of α–β PAC with block as a fixed effect in the model was not warranted ($\Delta AIC = -3$, $p > 0.1$, respectively). This indicated that despite variability in behavioral performance, the relationship between the behavioral precision as quantified by CV (Fig. 1*E*) and the strength of the α–β PAC was sustained throughout the entire experimental session. The lack of interaction precluded the possible confounding contribution of motivational or attentional effects typically observed as "time-on-task" effects. To further test whether PAC indexed the precision of behavioral performance, we assessed whether transitions in the strength of α–β PAC between blocks (ΔPAC) could predict transitions in behavioral precision between blocks (ΔCV). For this, we subtracted the CV and the α–β MI between consecutive blocks (i.e., Block 2 −

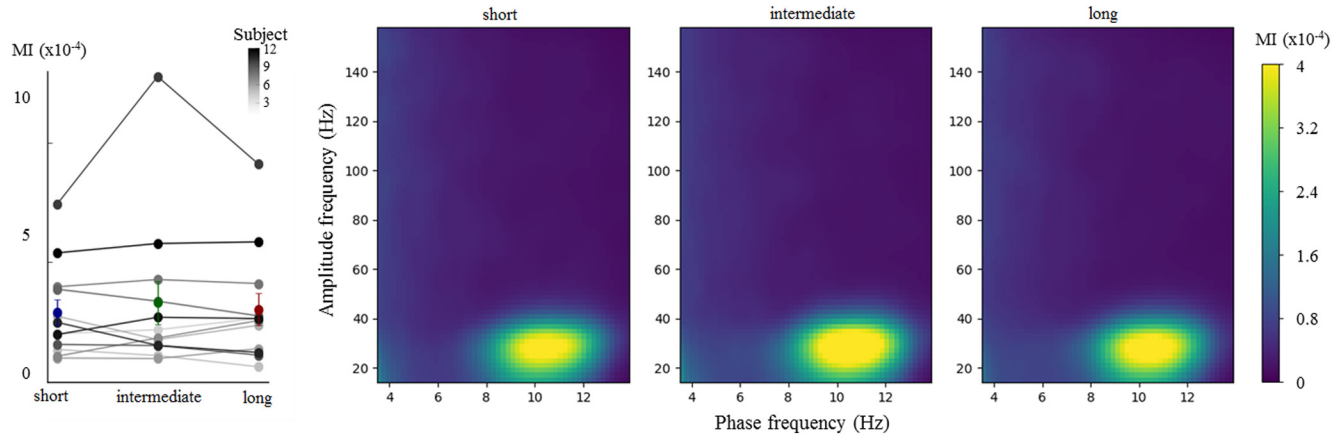

Figure 7. The strength of α–β coupling does not index absolute time production. Trials were split according to the length of the temporal production (left graph: gray, individual data; blue, green and red, mean and SEM for short, intermediate and long trials, respectively). A significant and comparable MI was found suggesting comparable α-β coupling whatever the length of the produced interval.

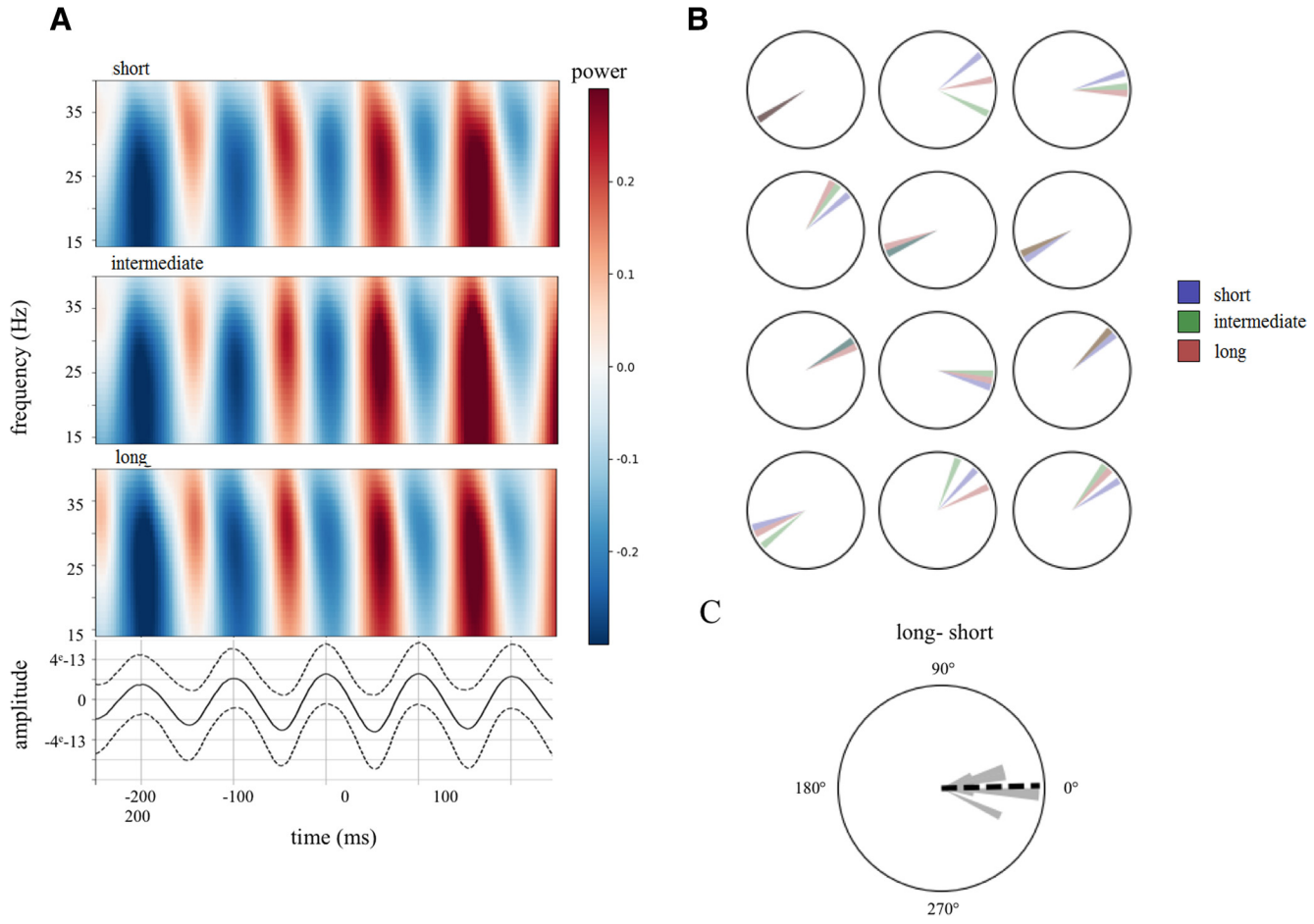

Figure 8. The relation between α phase and β power does not predict the length of produced temporal intervals. ***A***, The time series were locked on the peak of the α oscillations (bottom, dark line, SD marked by dashed lines) and beta power (15–40 Hz) were computed for each duration. For illustration, the time-frequency phase-locked to the α peak is shown for the MEG sensor showing maximal α–β MI for one representative participant (S06). ***B***, The α phase at which β power was maximal was extracted for each participant (circular histogram) and each duration category (blue, short; green, intermediate; red: long). ***C***, The α phase difference between long and short temporal productions at which β power was maximal was plotted for each participant. The length of the bar represents the number of participants with the same phase value. A Rayleigh test indicated that the phase difference between long and short categorizations was not uniform ($p < 0.02$, mean $= 1.4°$), confirming a significant phase concentration when beta power was maximal. However, the mean phase difference between long and short duration distribution did not significantly differ ($t = 0.12$, $p = 0.91$), providing no evidence for a different α–β phase relationship as a function of endogenous timing.

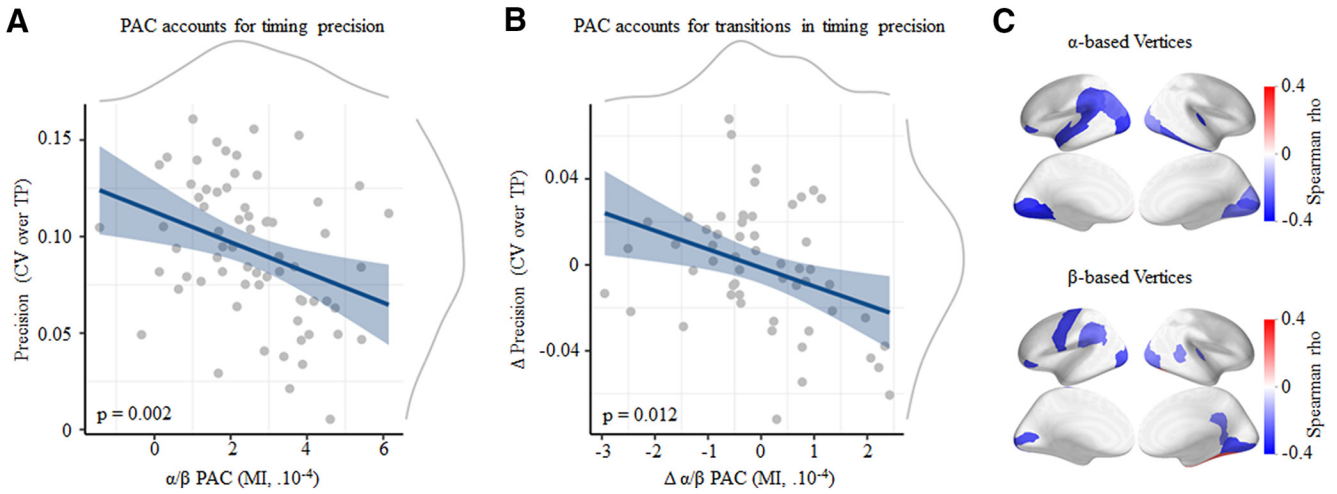

Figure 9. The strength of α–β PAC indexes the precision of temporal performance. ***A***, Over all experimental blocks and participants, CVs of temporal production were significantly correlated with the strength of α–β PAC. Additionally, α or β power showed no independent contribution to CV (Fig. 10), suggesting that α–β PAC exclusively accounted for participants' temporal precision. The shaded area around the regression line indicated standard error. ***B***, The relative changes in CV and α–β PAC were correlated when participants switched from one block to another, suggesting that the transitions in α–β coupling strength were associated with transitions in CV between blocks. The shaded area around the regression line indicated standard error. ***C***, Cortical source estimations of the correlations between α–β PAC and precision (CV). α–β PAC was calculated on the signal projected into source space. The correlations with CV were performed using Spearman's correlation. The blue areas indicate the labels that showed significant correlations.

Block 1, Block 3 − Block 2, etc.) and showed, in line with the results of the first model, that ΔPAC significantly predicted ΔCV ($t_{(51)} = 2.6$, $\beta = -77$, $p = 0.012$; Fig. 9*B*). This observation indicated that changes in precision (CV) between blocks could be accounted for by changes in the α–β coupling strength between blocks.

Previous studies on cross-frequency coupling have indicated that PAC estimation could be confounded during the estimation of phase and power frequencies (Aru et al., 2015). To thoroughly assess whether the predictive power of PAC strength with respect to behavioral CV was exclusive to oscillatory coupling, and not confounded by the power in α or β bands, we tested whether the inclusion of α power (Fig. 10*A*), β power (Fig. 10*B*), and α–β power ratio (Fig. 10*C*) was justified in the model predicting CV. We confirmed that the inclusion of α, β, and α–β ratio were not justified in the model predicting CV ($\Delta AIC = 1.2$, $p > 0.1$; $\Delta AIC = 1.8$, $p > 0.1$; $\Delta AIC = -2.9$, $p > 0.1$; respectively). The lack of predictability of precision by α and β power further supports that PAC is correlated with the precision in temporal performance, but also indicates that PAC is not caused by non-sinusoidal waveforms of α and/or β oscillations.

These series of tests were methodologically important to insure the biological reality and interpretation of PAC in our data. Indeed, the lack of correlation not only strengthened our previous observation that β oscillations were not harmonics of α but further supported the notion that PAC was not caused by non-sinusoidal waveforms of α and/or β oscillations (Cole and Voytek, 2017). In other words, these tests do not provide evidence for spurious PAC (Fig. 10).

Finally, we investigated the association between PAC and the precision of temporal behavior by correlating the values of the α–β MI obtained in each highlighted cortical region with the CVs: significant correlations between α–β MI and CV were found in the left motor cortices, in the left supramarginal gyrus, and in the occipito-parietal regions (Fig. 9*C*). Notably, the left supramarginal gyrus and pars orbitalis were conjointly seen in the α-based and in the β-based selection of vertices. The implication of these structures in the current timing task is consistent with previous reports (Coull et al., 2004; Livesey et al., 2007; Wiener et al., 2010).

The strength of α–β PAC and the power of α index temporal accuracy

The strength of α–β PAC was shown to correlate with the precision of temporal production (CV) across blocks with a stronger coupling indicating a smaller variance in time production. After investigating the *ad hoc* hypothesis proposing that PAC could regulate the precision of information processing, we assessed whether α–β PAC was also related to the differences between produced time intervals, and the objective target intervals, i.e., to the accuracy quantified as ERs.

The ER indicated the distance of participants' temporal production from an ideal observer's performance (Fig. 1*D*). We found that the strength of α–β PAC was approaching significance in predicting ER ($t_{(58)} = 1.9$, $\beta = -44$, $p = 0.058$; Fig. 11). The AIC analysis showed that the model containing the strength of α–β PAC as predictor was marginally justified compared with the model including only the intercept ($\Delta AIC = 1.7$, $p = 0.055$). No interaction between the strength of α–β PAC and block as fixed effect was found ($\Delta AIC = 2.8$, $p > 0.1$) by comparing a model with α–β PAC as a single predictor and a model in which interaction with block was added. This result signified that the changes in behavioral feedback to the participant did not affect the strength in α–β coupling. This was further verified by directly contrasting blocks containing feedback on all trials (100% feedback) with blocks in which participants received feedback in only 15% of the trials. The inclusion of feedback in the model was not warranted ($\Delta AIC = 0.5$, $p > 0.1$). It thus appeared that the relationship between the observed oscillatory coupling strength, as measured by α–β PAC, and the accuracy of time estimation, as measured by ER, remained stable throughout the entire experimental session.

Finally, to assess the relative contribution of precision and accuracy in relation to α–β PAC, we performed a series of model comparison with precision and accuracy as predictors, again keeping the same random structure as in the previous statistical

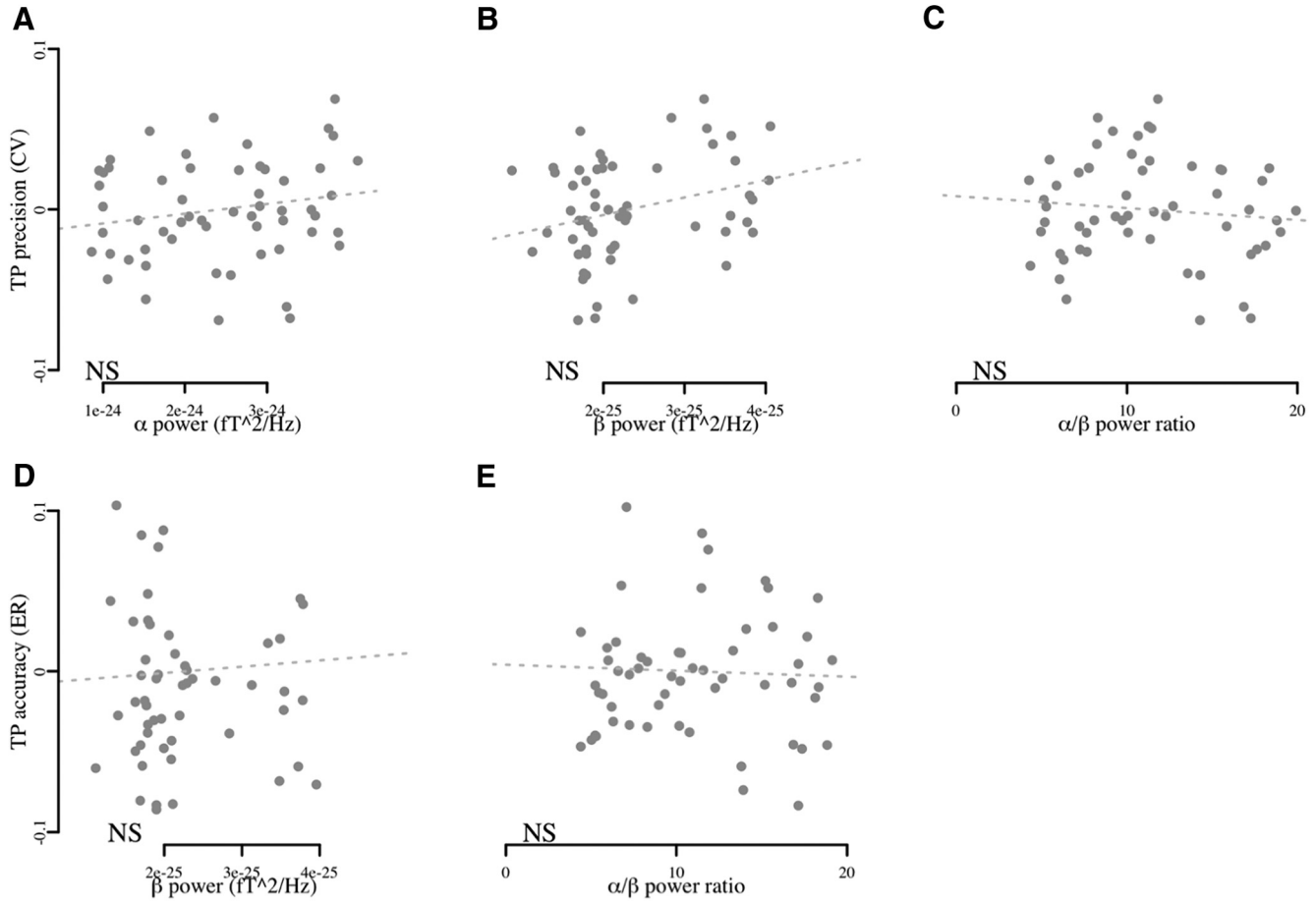

Figure 10. α And β power do not independently contribute to the precision in temporal performance. Over all blocks and participants, the CVs of time interval did not significantly correlate with the strength of α or β power or their ratio (***A–C***, respectively). In the absence of significant contributions of α or β power to ER in TP (***D***, ***E***, respectively), TP did not correlate with the strength of β power or α–β power ratio. This set of results further strengthens the finding that it is the coupling of α–β, and not α or β alone that contribute to temporal precision.

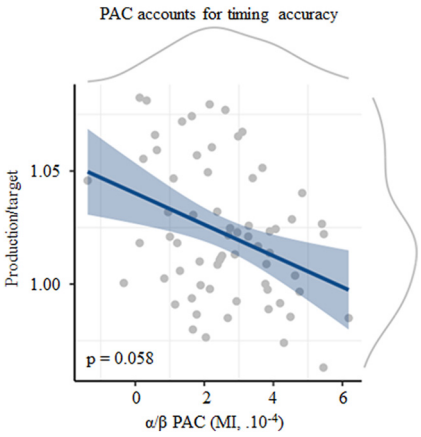

Figure 11. α–β PAC index performance accuracy. A decrease in ER of time production was near significantly correlated with a decrease in α–β coupling strength. The shaded area around the regression line indicated standard error.

assessments. First, we compared the model including CV against the model including CV and ER. The addition of ER in the model was not justified (ΔAIC = 0.3, $p > 0.1$). However, comparison of the model including ER against the model including ER and CV showed that inclusion of CV was justified (ΔAIC = 0.3, $p > 0.1$). Together, this indicated that precision (CV) accounted for the part of the variance that was targeted by near significant effect of accuracy.

Altogether, and in line with the outcomes of the precision model, the accuracy model showed that a decrease in the strength of α–β coupling predicted less accurate time productions. At first, the functional role of α–β PAC on accuracy seemed less clear than the one of precision; however, we contend that the decrease in accuracy could result from the loss of precision, with an increased likelihood of poorer time estimation supported by model comparisons investigating the relative contributions of CV and ER in explaining α–β PAC. All in all, our results provide no evidence for a specific role of cross-frequency coupling in duration estimation per se, but rather suggests that the strength of α–β oscillatory coupling indexes the precision with which endogenous temporal goals may be maintained across trials (Fig. 12). We discuss in the next section one interpretation, in which, from a neural network perspective, α oscillations may be regulating the β timing goal generated endogenously.

Discussion

Using time-resolved neuroimaging, we investigated whether cross-frequency coupling participates in the endogenous generation of time intervals. Our results provide evidence that the strength of α–β PAC may leverage the precision, but not the coding, of a time interval. Specifically, we found that the strength of α–β PAC was indicative of the precision of endogenous timing, so that the stronger the α–β coupling, the more precise the

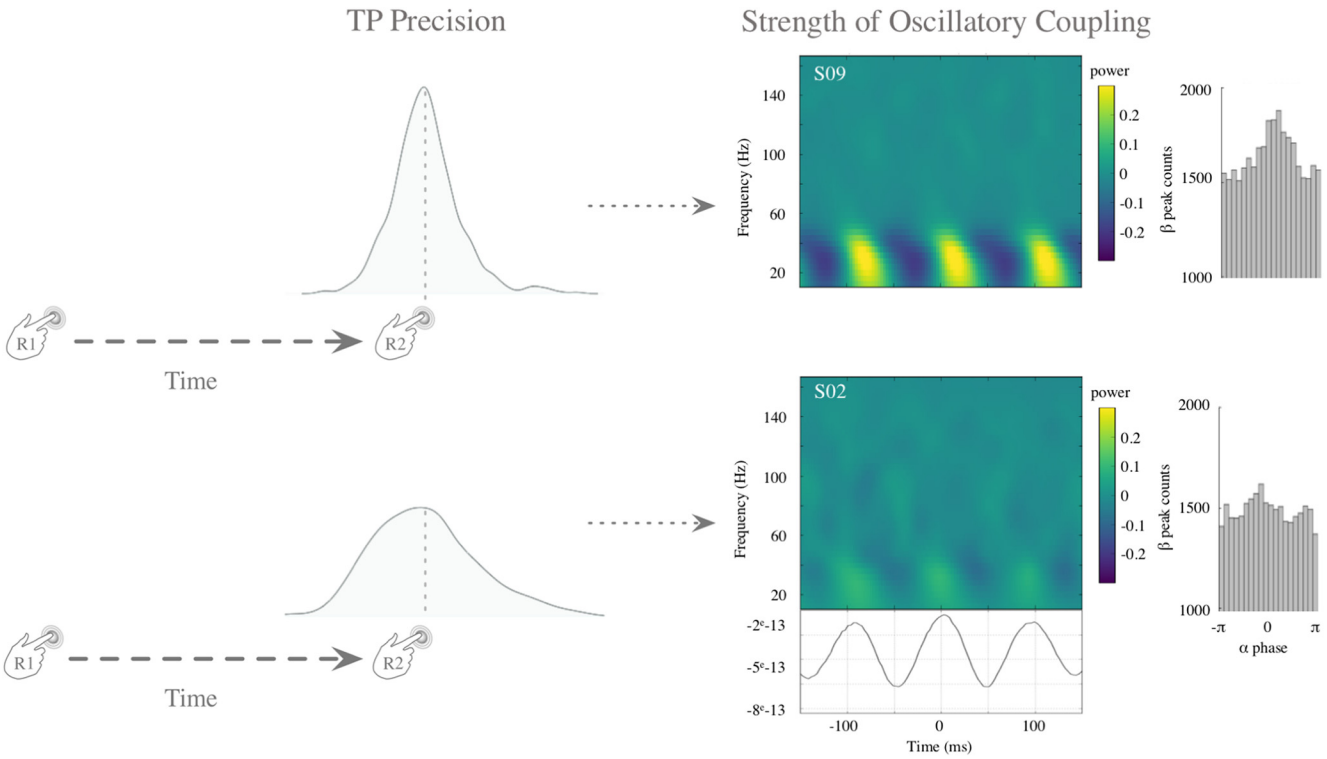

Figure 12. The strength of α–β oscillatory coupling regulates timing precision. An individual's precision in a TP task may depend on the strength of α–β PAC. Higher precision corresponds to a narrower distribution of temporal productions (top left; behavioral data for individual S09), whereas a lower precision corresponds to a broader distribution of temporal productions (bottom left, behavioral data for individual S02). Right, Time-frequency plots of the mean β power time-locked to the phase of α (here, the peak). For one individual with high behavioral precision (S09; top), a strong α–β PAC can be seen. The peak count distribution of β power maxima relative to the α phase that are provided on the right shows, for individual S09, a strong concentration of maximal β power with the α phase. Conversely, for the individual with lower behavioral precision (S02; bottom), a weaker α–β PAC was found: the peak count distribution of β power maxima relative to the α phase for this individual showed a flatter distribution indicated a lower dependency of β power maxima on α phase.

performance (Fig. 9). These results suggest that α–β coupling indexes the precision with which information may be endogenously maintained, and transferred, within brain networks during an endogenous cognitive task.

α–β PAC is not related to motor preparation or learning

Accounting for the present findings with existing evidence for the implication of PAC in motor preparation and learning would be tempting but several results suggest that this may not be the case here. First, none of the frequency regimes in our study conformed to previous reports: for instance, in intracranial recordings and electrocorticography, motor preparation induced coupling in α-high γ with an enhanced coupling during the preparation compared with the movement execution (Yanagisawa et al., 2012; Combrisson et al., 2017). Additionally, δ–α PAC contralateral to the side of the motor preparation was found to increase during movement versus no movement (Kajihara et al., 2015). In situations of aberrant oscillatory regimes, such as in patients with Parkinson, de Hemptine et al. (2015) described an increased β-high γ PAC. Although we cannot be fully exhaustive, motor functions have typically been linked to other frequency coupling than the α–β PAC observed here.

Another line of research reported the enhancement of PAC during learning (Tort et al., 2009), understood as a progressive improvement in the measured neural or behavioral feature over the course of the experiment (Tort et al., 2009; Kononowicz and Van Rijn, 2011). In our study, participants' behavioral precision was stable over experimental blocks, suggesting no effect of practice or learning in the course of the experiment. Additionally, the association between the strength of α–β PAC with behavioral precision was stable over blocks. It would thus be presently difficult to interpret our results in the context of learning (Tort et al., 2009). Although different durations may entail different working memory loads, we also did not find any increase in the strength of PAC with the length of duration. As our experimental design did not explicitly manipulate learning or memory during time production, we cannot fully conclude on their possible interactions with the reported effect and these aspects would be helpful to manipulate in future work.

Maintenance of an endogenous temporal goal through α–β coupling

The specific role of α oscillations in cognition and information processing remains largely debated (Roux and Uhlhaas, 2014) but several observations show some consistencies. Among them, α oscillations have seminally been associated with the inhibition of irrelevant information (Klimesch et al., 2007; Jensen and Mazaheri, 2010; Haegens et al., 2012) and the maintenance of contents in working memory (Bonnefond and Jensen, 2012). The power of α oscillations has been shown to increase during cognitive tasks requiring internal engagement, which supports the protective role of α rhythms against exogenous distraction (Scheeringa et al., 2009). α Oscillations have also been shown to play an active role in working memory maintenance (Palva and Palva, 2011) and in anticipation (Haegens et al., 2012; Praamstra et al., 2006). Both anticipation (Fortin and Massé, 2000; Fortin et al., 2005; Coull et al., 2013) and maintenance of task goal (Lustig and Meck, 2001) are vital functions in time estimation. Hence,

our observation of an active engagement of α oscillations in this task is consistent with prior literature.

β Oscillations have been implicated in the generation of temporal predictions through sensorimotor interactions (Fujioka et al., 2012; Arnal et al., 2014) and in the encoding of inter-tap duration (Bartolo and Merchant, 2015). β Oscillations have been proposed to index a neural code for time estimation during motor timing (Kononowicz et al., 2018) and perceptual timing (Kulashekhar et al., 2016), with β power linearly increasing with time estimates (but see Ghaderi et al., 2018). A causal link between β power and time estimation has recently been established (Wiener et al., 2018). Hence, the active implication of β oscillations in our task is largely consistent with prior literature.

In line with the proposal that α and β regimes cooperate for content maintenance (Palva and Palva, 2007), α-driven PAC could provide a computational framework, in which α rhythms serve as a readout for relevant items (Nikulin and Brismar, 2006; Roux and Uhlhaas, 2014). Our time production paradigm relied on the anticipation of internally generated temporal codes (and volitional goals; Haggard, 2008, 2017) for duration production and PAC has also been reported during externally driven anticipatory states (Cohen et al., 2009; Cravo et al., 2011). The observation that enhanced PAC would index more precise temporal productions across blocks is consistent with the idea that coupled neuronal regimes contribute to the selection and the maintenance of neuronal representations (Palva and Palva, 2007). Given that α–β PAC was commensurate with the endogenous precision of a time goal, one hypothesis we would like to put forward is that β-based event computations may support endogenous temporal codes (and timed actions).

Specificity of α–β coupling to the precision of motor timing in the absence of external stimulation

A large body of work has suggested that PAC plays a functional role in maintaining information in working-memory and in attention. In working memory, PAC operate in the θ–γ regimes (Axmacher et al., 2010; Fell and Axmacher, 2011; Alekseichuk et al., 2016), whereas modulations of attention entail the α–γ regimes (Voytek et al., 2010; Roux and Uhlhaas, 2014). An enhanced PAC has been associated with increased working-memory load (Axmacher et al., 2010) and successful memory recollection in a cued task (Park et al., 2016). In both cases, γ activity was reported as the oscillatory component underlying information maintenance in working memory (Herrmann et al., 2004; but see Daume et al., 2017). The integration hypothesis predicted an increased strength of oscillatory coupling as a function of the length of the estimated duration but we found no compelling evidence for it. Our results seemed more consistent with the precision hypothesis, and with two studies showing a phase alignment of slow oscillations with the temporal task structure (Cravo et al., 2011; Samaha et al., 2015; Mento et al., 2018). For instance, Cravo et al. (2011) reported increased PAC between two moments in time (temporal expectancy) for which it was perceptually beneficial for participants to maintain the same anticipation level. Both paradigms (Cravo et al., 2011; Samaha et al., 2015) relied on an individual's anticipation of external sensory inputs, supporting the notion that anticipatory states could be maintained through α–β PAC. Our results extend these observations by showing that α–β PAC is relevant for precision in motor timing and with recent observations that the precision of neural representations may rely on multiple oscillators (Kheifets et al., 2017).

It is also noteworthy that exogenous sensory entrainment implicates the coupling of β oscillations with delta (δ; 1–3 Hz) unlike the self-generated and endogenous α–β coupling: δ–β PAC was observed during the anticipation of visual sequences (Saleh et al., 2010) and linked to the temporal resolution of perceptual systems (Arnal et al., 2014). High δ–β coupling has been associated with temporally accurate perception of an auditory stimulus embedded within a sequence (Arnal et al., 2014), and changes in the phase of δ oscillations, associated with explicit time order (Kösem et al., 2014).

α–β PAC as a signature of neural stabilization

α–β PAC has rarely been explored as a coupling configuration (Canolty et al., 2010; Hyafil et al., 2015), but our results highlight a couple interesting features. First, α and β generating networks appear, to a certain extent, intertwined during a volitional task engaging no sensory stimulation (i.e., self-generated endogenous timing). Second, that higher precision may arise from the maintenance of β-encoded information by the phase of α rhythm is in line with recent simulations using a four-layer neuronal mass model (Sotero, 2015, 2016). The phase of α oscillations may provide an optimal window for the reactivation of β-driven activity, consistent with a global α network regulating local β activity (Lee et al., 2013). This interpretation would also be in line with the suggestion that β synchronization provides a functional assembly-forming mechanism (Lundqvist et al., 2016; Spitzer and Haegens, 2017). In this broad context, α–β PAC as a marker of precision signifies that, in the absence of updating of the synaptic weights, the endogenous temporal goal may drift away from the optimal space (Kononowicz et al., 2018).

Conclusions

We report that the strength of α–β PAC varied as a function of the precision with which participants generated a time interval. Oscillatory coupling was robustly found in each individual during a volitional motor timing task. We suggest that α oscillations maintain and support the organization of β oscillations to keep track of endogenous temporal goals. Our results provide strong evidence that α–β PAC leverages the precision of timing, but not absolute timing itself.

References

Akam T, Kullmann DM (2014) Oscillatory multiplexing of population codes for selective communication in the mammalian brain. Nat Rev Neurosci 15:111–122.

Alekseichuk I, Turi Z, Amador de Lara G, Antal A, Paulus W (2016) Spatial working memory in humans depends on theta and high gamma synchronization in the prefrontal cortex. Curr Biol 26:1513–1521.

Arnal LH, Doelling KB, Poeppel D (2014) Delta–beta coupled oscillations underlie temporal prediction accuracy. Cereb Cortex 25:3077–3085.

Aru J, Aru J, Priesemann V, Wibral M, Lana L, Pipa G, Singer W, Vicente R (2015) Untangling cross-frequency coupling in neuroscience. Curr Opin Neurobiol 31:51–61.

Axmacher N, Henseler MM, Jensen O, Weinreich I, Elger CE, Fell J (2010) Cross-frequency coupling supports multi-item working memory in the human hippocampus. Proc Natl Acad Sci U S A 107:3228–3233.

Bartolo R, Merchant H (2015) β oscillations are linked to the initiation of sensory-cued movement sequences and the internal guidance of regular tapping in the monkey. J Neurosci 35:4635–4640.

Bonnefond M, Jensen O (2012) Alpha oscillations serve to protect working memory maintenance against anticipated distracters. Curr Biol 22:1969–1974.

Brainard DH (1997) The psychophysics toolbox. Spat Vis 10:433–436.

Buzsáki G (2010) Neural syntax: cell assemblies, synapsembles, and readers. Neuron 68:362–385.

Buzsáki G, Draguhn A (2004) Neuronal oscillations in cortical networks. Science 304:1926–1929.
Canolty RT, Knight RT (2010) The functional role of cross-frequency coupling. Trends Cogn Sci 14:506–515.
Canolty RT, Edwards E, Dalal SS, Soltani M, Nagarajan SS, Kirsch HE, Berger MS, Barbaro NM, Knight RT (2006) High gamma power is phase-locked to theta oscillations in human neocortex. Science 313:1626–1628.
Cohen MX, Axmacher N, Lenartz D, Elger CE, Sturm V, Schlaepfer TE (2009) Good vibrations: cross-frequency coupling in the human nucleus accumbens during reward processing. J Cogn Neurosci 21:875–889.
Cole SR, Voytek B (2017) Brain oscillations and the importance of waveform shape. Trends Cogn Sci 21:137–149.
Combrisson E, Perrone-Bertolotti M, Soto JL, Alamian G, Kahane P, Lachaux JP, Guillot A, Jerbi K (2017) From intentions to actions: neural oscillations encode motor processes through phase, amplitude and phase-amplitude coupling. Neuroimage 147:473–487.
Coull JT, Vidal F, Nazarian B, Macar F (2004) Functional anatomy of the attentional modulation of time estimation. Science 303:1506–1508.
Coull JT, Davranche K, Nazarian B, Vidal F (2013) Functional anatomy of timing differs for production versus prediction of time intervals. Neuropsychologia 51:309–319.
Cravo AM, Rohenkohl G, Wyart V, Nobre AC (2011) Endogenous modulation of low-frequency oscillations by temporal expectations. J Neurophysiol 106:2964–2972.
Dale AM, Liu AK, Fischl BR, Buckner RL, Belliveau JW, Lewine JD, Halgren E (2000) Dynamic statistical parametric mapping: combining fMRI and MEG for high-resolution imaging of cortical activity. Neuron 26:55–67.
Daume J, Gruber T, Engel AK, Friese U (2017) Phase–amplitude coupling and long-range phase synchronization reveal frontotemporal interactions during visual working memory. J Neurosci 37:313–322.
de Hemptine C, Swann NC, Ostrem JL, Ryapolova-Webb ES, San Luciano M, Galifianakis NB, Starr PA (2015) Therapeutic deep brain stimulation reduces cortical phase-amplitude coupling in Parkinson's disease. Nat Neurosci 18:779–786.
Desikan RS, Ségonne F, Fischl B, Quinn BT, Dickerson BC, Blacker D, Buckner RL, Dale AM, Maguire RP, Hyman BT, Albert MS, Killiany RJ (2006) An automated labeling system for subdividing the human cerebral cortex on MRI scans into gyral based regions of interest. Neuroimage 31:968-980.
Dupré la Tour T, Tallot L, Grabot L, Doyère V, van Wassenhove V, Grenier Y, Gramfort A (2017) Non-linear auto-regressive models for cross-frequency coupling in neural time series. PLoS Comput Biol 13:e1005893.
Fell J, Axmacher N (2011) The role of phase synchronization in memory processes. Nat Rev Neurosci 12:105–118.
Fischl B, Salat DH, van der Kouwe AJ, Makris N, Ségonne F, Quinn BT, Dale AM (2004) Sequence-independent segmentation of magnetic resonance images. Neuroimage 23:S69–S84.
Fortin C, Massé N (2000) Expecting a break in time estimation: attentional time-sharing without concurrent processing. J Exp Psychol Hum Percept Perform 26:1788–1796.
Fortin C, Bédard MC, Champagne J (2005) Timing during interruptions in timing. J Exp Psychol Hum Percept Perform 31:276–288.
Fries P (2015) Rhythms for cognition: communication through coherence. Neuron 88:220–235.
Fujioka T, Trainor LJ, Large EW, Ross B (2012) Internalized timing of isochronous sounds is represented in neuromagnetic β oscillations. J Neurosci 32:1791–1802.
Ghaderi AH, Moradkhani S, Haghighatfard A, Akrami F, Khayyer Z, Balcı F (2018) Time estimation and beta segregation: an EEG study and graph theoretical approach. PLoS One 13: e0195380.
Gelman A, Hill J (2007) Data analysis using regression and hierarchical/multilevel models. New York, NY: Cambridge.
Giraud AL, Poeppel D (2012) Cortical oscillations and speech processing: emerging computational principles and operations. Nat Neurosci 15: 511–517.
Goerg GM (2011) Lambert W random variables: a new family of generalized skewed distributions with applications to risk estimation. Ann Appl Stat 5:2197–2230.
Goerg GM (2015) The lambert way to Gaussianize heavy-tailed data with the inverse of Tukey's h transformation as a special case. ScientificWorldJournal 2015:909231.
Gramfort A, Luessi M, Larson E, Engemann DA, Strohmeier D, Brodbeck C, Goj R, Jas M, Brooks T, Parkkonen L, Hämäläinen M (2013) MEG and EEG data analysis with MNE-Python. Front Neurosci 7:267.
Gramfort A, Luessi M, Larson E, Engemann DA, Strohmeier D, Brodbeck C, Parkkonen L, Hämäläinen MS (2014) MNE software for processing MEG and EEG data. Neuroimage 86:446–460.
Green P, MacLeod CJ (2016) SIMR: an R package for power analysis of generalized linear mixed models by simulation. Methods Ecol Evol 7:493–498.
Gu BM, van Rijn H, Meck WH (2015) Oscillatory multiplexing of neural population codes for interval timing and working memory. Neurosci Biobehav Rev 48:160–185.
Haegens S, Luther L, Jensen O (2012) Somatosensory anticipatory alpha activity increases to suppress distracting input. J Cogn Neurosci 24:677–685.
Haggard P (2008) Human volition: towards a neuroscience of will. Nat Rev Neurosci 9:934–946.
Haggard P (2017) Sense of agency in the human brain. Nat Rev Neurosci 18:196–207.
Heusser AC, Poeppel D, Ezzyat Y, Davachi L (2016) Episodic sequence memory is supported by a theta-gamma phase code. Nat Neurosci 19: 1374–1380.
Herrmann CS, Munk MH, Engel AK (2004) Cognitive functions of gamma-band activity: memory match and utilization. Trends Cogn Sci 8:347–355.
Hyafil A, Giraud AL, Fontolan L, Gutkin B (2015) Neural cross-frequency coupling: connecting architectures, mechanisms, and functions. Trends Neurosci 38:725–740.
Jacobs J, Kahana MJ, Ekstrom AD, Fried I (2007) Brain oscillations control timing of single-neuron activity in humans. J Neurosci 27:3839–3844.
Jeffreys H (1961) Theory of probability, Ed 3. Oxford, UK: Clarendon.
Jensen O, Colgin LL (2007) Cross-frequency coupling between neuronal oscillations. Trends Cogn Sci 11:267–269.
Jensen O, Mazaheri A (2010) Shaping functional architecture by oscillatory alpha activity: gating by inhibition. Front Hum Neurosci 4:186.
Jovicich J, Czanner S, Greve D, Haley E, van der Kouwe A, Gollub R, Kennedy D, Schmitt F, Brown G, Macfall J, Fischl B, Dale A (2006) Reliability in multi-site structural MRI studies: effects of gradient non-linearity correction on phantom and human data. Neuroimage 30:436–443.
Kajihara T, Anwar MN, Kawasaki M, Mizuno Y, Nakazawa K, Kitajo K (2015) Neural dynamics in motor preparation: from phase-mediated global computation to amplitude-mediated local computation. Neuroimage 118:445–455.
Kheifets A, Freestone D, Gallistel CR (2017) Theoretical implications of quantitative properties of interval timing and probability estimation in mouse and rat. J Exp Anal Behav 108:39–72.
Klimesch W, Sauseng P, Hanslmayr S (2007) EEG alpha oscillations: the inhibition–timing hypothesis. Brain Res Rev 53:63–88.
Kononowicz TW, Penney TB (2016) The contingent negative variation (CNV): timing isn't everything. Curr Opin Behav Sci 8:231–237.
Kononowicz TW, van Rijn H (2015) Single trial beta oscillations index time estimation. Neuropsychologia 75:381–389.
Kononowicz TW, van Rijn H (2011) Slow potentials in time estimation: the role of temporal accumulation and habituation. Front Integr Neurosci 5:48.
Kononowicz, van Wassenhove V (2016) In search of oscillatory traces of the internal clock. Front Psychol 7:224.
Kononowicz TW, Roger C, van Wassenhove V (2018) Temporal metacognition as the decoding of self-generated brain dynamics. Cereb Cortex. Advance online publication. Retrieved December 22, 2018. doi: 10.1093/cercor/bhy318.
Kösem A, Gramfort A, van Wassenhove V (2014) Encoding of event timing in the phase of neural oscillations. Neuroimage 92: 274–284.
Kulashekhar S, Pekkola J, Palva JM, Palva S (2016) The role of cortical beta oscillations in time estimation. Hum Brain Mapp 37:3262–3281.
Kuznetsova A, Brockhoff PB, Christensen R HB (2017) lmerTest package: tests in linear mixed effects models. Journal of Statistical Software 82: 1–26.
Lee JH, Whittington MA, Kopell NJ (2013) Top-down beta rhythms support selective attention via interlaminar interaction: a model. PLoS Comput Biol 9:e1003164.
Lee MD, Wagenmakers EJ (2014) Bayesian cognitive modeling: a practical course. New York: Cambridge UP.
Lisman JE, Jensen O (2013) The theta-gamma neural code. Neuron 77: 1002–1016.

Livesey AC, Wall MB, Smith AT (2007) Time perception: manipulation of task difficulty dissociates clock functions from other cognitive demands. Neuropsychologia 45:321–331.

Lundqvist M, Rose J, Herman P, Brincat SL, Buschman TJ, Miller EK (2016) Gamma and beta bursts underlie working memory. Neuron 90:152–164.

Lustig C, Meck WH (2001) Paying attention to time as one gets older. Psychol Sci 12:478–484.

Mento G, Astle DE, Scerif G (2018) Cross-frequency phase–amplitude coupling as a mechanism for temporal orienting of attention in childhood. J Cogn Neurosci 30:594–602.

Mita A, Mushiake H, Shima K, Matsuzaka Y, Tanji J (2009) Interval time coding by neurons in the presupplementary and supplementary motor areas. Nat Neurosci 12:502–507.

Nikulin VV, Brismar T (2006) Phase synchronization between alpha and beta oscillations in the human electroencephalogram. Neuroscience 137:647–657.

Palva S, Palva JM (2007) New vistas for α-frequency band oscillations. Trends Neurosci 30:150–158.

Palva S, Palva JM (2011) Functional roles of alpha-band phase synchronization in local and large-scale cortical networks. Front Psychol 2:204.

Park H, Lee DS, Kang E, Kang H, Hahm J, Kim JS, Chung CK, Jiang H, Gross J, Jensen O (2016) Formation of visual memories controlled by gamma power phase-locked to alpha oscillation. Sci Rep 6:28092.

Pinheiro JC, Bates DM (2000) Linear mixed-effects models: basic concepts and examples. In: Mixed-effects models in S and S-Plus. Statistics and Computing, pp 3–56. New York, NY:Springer.

Praamstra P, Kourtis D, Kwok HF, Oostenveld R (2006) Neurophysiology of implicit timing in serial choice reaction-time performance. J Neusci 26: 5448–5455.

R Core Team (2016) R: A language and environment for statistical computing. Vienna: R Foundation for Statistical Computing.

Rouder JN, Morey RD, Speckman PL, Province JM (2012) Default bayes factors for ANOVA designs. J Math Psychol 56:356–374.

Roux F, Uhlhaas PJ (2014) Working memory and neural oscillations: alpha–gamma versus theta–gamma codes for distinct WM information? Trends Cogn Sci 18:16–25.

Saleh M, Reimer J, Penn R, Ojakangas CL, Hatsopoulos NG (2010) Fast and slow oscillations in human primary motor cortex predict oncoming behaviorally relevant cues. Neuron 65:461–471.

Samaha J, Bauer P, Cimaroli S, Postle BR (2015) Top-down control of the phase of alpha-band oscillations as a mechanism for temporal prediction. Proc Natl Acad Sci U S A 112:8439–8444.

Scheeringa R, Petersson KM, Oostenveld R, Norris DG, Hagoort P, Bastiaansen MC (2009) Trial-by-trial coupling between EEG and BOLD identifies networks related to alpha and theta EEG power increases during working memory maintenance. Neuroimage 44:1224–1238.

Sotero RC (2015) Modeling the generation of phase-amplitude coupling in cortical circuits: from detailed networks to neural mass models. Biomed Res Int 2015:915606.

Sotero RC (2016) Topology, cross-frequency, and same-frequency band interactions shape the generation of phase-amplitude coupling in a neural mass model of a cortical column. PLoS Comput Biol 12:e1005180.

Spitzer B, Haegens S (2017) Beyond the status quo: a role for beta oscillations in endogenous content (re-) activation. eNeuro 4:ENEURO-0170-17.2017.

Tort AB, Kramer MA, Thorn C, Gibson DJ, Kubota Y, Graybiel AM, Kopell NJ (2008) Dynamic cross-frequency couplings of local field potential oscillations in rat striatum and hippocampus during performance of a *t*-maze task. Proc Natl Acad Sci U S A 105:20517–20522.

Tort AB, Komorowski RW, Manns JR, Kopell NJ, Eichenbaum H (2009) Theta–gamma coupling increases during the learning of item–context associations. Proc Natl Acad Sci U S A 106:20942–20947.

Tort AB, Komorowski R, Eichenbaum H, Kopell N (2010) Measuring phase-amplitude coupling between neuronal oscillations of different frequencies. J Neurophysiol 104:1195–1210.

Treisman M (1963) Temporal discrimination and the indifference interval: Implications for a model of the "internal clock". Psychol Monogr 77:1–31.

van Wassenhove V (2016) Temporal cognition and neural oscillations. Curr Opin Behav Sci 8:124–130.

Voytek B, Canolty RT, Shestyuk A, Crone NE, Parvizi J, Knight RT (2010) Shifts in gamma phase–amplitude coupling frequency from theta to alpha over posterior cortex during visual tasks. Front Hum Neurosci 4:191.

Wagenmakers EJ, Farrell S (2004) AIC model selection using akaike weights. Psychon Bull Rev 11:192–196.

Wiener M, Parikh A, Krakow A, Coslett HB (2018) An intrinsic role of beta oscillations in memory for time estimation. Sci Rep 8:7992.

Wiener M, Hamilton R, Turkeltaub P, Matell MS, Coslett HB (2010) Fast forward: supramarginal gyrus stimulation alters time measurement. J Cogn Neurosci 22:23–31.

Yanagisawa T, Yamashita O, Hirata M, Kishima H, Saitoh Y, Goto T, Yoshimine T, Kamitani Y (2012) Regulation of motor representation by phase–amplitude coupling in the sensorimotor cortex. J Neurosci 32: 15467–15475.